Diffusion or advection? Mass transfer and diffusive boundary layer landscapes of the brown alga *Fucus vesiculosus*

Mads Lichtenberg[a,1,2]; mads.lichtenberg@bio.ku.dk, +45 3533 0185

Rasmus Dyrmose Nørregaard[b,1]; rdyn@bios.au.dk

Michael Kühl[a,c]; mkuhl@bio.ku.dk

[a] Marine Biological Section, Department of Biology, University of Copenhagen, Strandpromenaden 5, DK-3000 Helsingør, Denmark.

[b] Arctic Research Center, Department of Bioscience, Faculty of Science and Technology, Aarhus University, Frederiksborgvej 399, 4000 Roskilde, Denmark.

[c] Climate Change Cluster, University of Technology Sydney, PO Box 123, Ultimo Sydney NSW 2007, Australia.

Running title: DBL landscapes around *Fucus vesiculosus*

[1] These authors contributed equally to this work

[2] Corresponding author,

Abstract

The role of hyaline hairs on the thallus of brown-algae in the genus *Fucus* is long debated and several functions have been proposed. We used a novel motorized setup for 2D- and 3D-mapping with O_2-microsensors to investigate the spatial heterogeneity of the diffusive boundary layer (DBL) and O_2 flux around single and multiple tufts of hyaline hairs on the thallus of *Fucus vesiculosus*. Flow was a major determinant of DBL thickness, where higher flow decreased DBL thickness and increased O_2 flux between algal thallus and the surrounding seawater. However, the topography of the DBL varied and did not directly follow the contour of the underlying thallus. Areas around single tufts of hyaline hairs exhibited both increased and decreased DBL thickness as compared to areas over smooth thallus surfaces. Over thallus areas with several hyaline hair tufts, the overall effect was a local increase in the DBL thickness. We also found indications for advective O_2 transport driven by pressure gradients or vortex-shedding downstream from dense tufts of hyaline hairs alleviating local mass-transfer resistance imposed by thickened DBL. Mass-transfer dynamics around hyaline hair tufts are thus more complex than hitherto assumed and may have important implications for algal physiology and plant-microbe interactions.

Keywords: biological fluid mechanics, diffusive boundary layer, macroalgae, mass transfer, oxygen, topography.

Introduction

Aquatic macrophytes are limited compared to their terrestrial counterparts by the ~10^4 slower diffusion and a much lower solubility of gases in water than in air [1, 2]. The efficient exchange of nutrients and gases is further exacerbated by the diffusive boundary layer (DBL) surrounding all submersed surfaces [3]. The thickness and topography of diffusive boundary layers around submerged impermeable objects is affected by flow velocity and surface topography [3]. Higher flow velocities decrease the DBL thickness by exerting a higher shear stress on the viscous sublayer near the surface. The effect of surface roughness on DBL thickness is variable, where angled planes facing the flow generally will have decreased boundary layers, while the DBL downstream of protruding structures will have increased boundary layers. At the same time, the effect of surface roughness on mass transfer across a boundary layer is dichotomous, where a thicker DBL will decrease mass transfer, while surface roughness tends to increase the overall surface area increasing mass transfer [3]. In microsensor-based studies of the DBL, it is important to note that the presence of the microsensor tip in itself can affect the local DBL thickness [4], where flow acceleration around the microsensor shaft will compress the local DBL thickness leading to locally enhanced O_2 fluxes in the order of 10%. However, this effect is only significant when investigated on smooth surfaces, while a clear effect is apparently undetectable when measured over tufts in e.g. a cyanobacterial mat [5].

It has been estimated that the DBL accounts for up to 90% of the resistance to carbon fixation in freshwater plants [6], and structural- and biochemical regulations to alleviate such mass transfer resistance have evolved across lineages. Some aquatic macrophytes have e.g. developed i) thinner leaves and a reduced cuticle that decreases the diffusion path length to chloroplasts, ii) carbon concentrating mechanisms that increase internal carbon concentration, and iii) the ability to utilize HCO_3^- which constitutes the largest fraction of dissolved inorganic carbon at ocean pH ([7], [8] and references therein). In photosymbiotic corals it has also been proposed that vortical ciliary flow can actively enhance mass transfer between the coral tissue and the surrounding water in stagnant or very low flow regimes with concomitant thick diffusive boundary layers [9].

Hyaline hairs, i.e., colourless, filamentous multicellular structures, are often observed as whitish tufts on the thallus of brown macroalgae in the genus *Fucus*. The hairs originate and are anchored in cryptostomatal cavities on the apical- and mid-regions of the thallus

[10]. It is recognized that hyaline hairs aid in the uptake of nutrients [11, 12] e.g. during springtime, when photosynthetic potential is higher due to increased light levels and the need for nutrients apparently triggers growth of hyaline hairs [10].

How hyaline hairs affect solute exchange and nutrient acquisition in *Fucus* is still debated, although a number of suggestions currently exist in the literature suggesting that: i) the hairs increase the algal surface area available for nutrient uptake, albeit this is probably not the major limitation on nutrient uptake [11]; ii) the hyaline hairs might decrease the diffusive boundary layer (DBL) due to turbulence created by the hairs as water flows across them, decreasing the mass resistance imposed by the DBL [11]; iii) the thin cell walls of the hairs relative to the thallus could have less resistance to the passage of ions [13, 14]; iv) the hyaline hairs increase DBL thickness, thereby retaining the products of thallus surface-active enzymes such as extracellular phosphatases and ensuring more efficient nutrient uptake [14].

There can be no doubt, however, that the DBL has great importance for macroalgal growth rates. The mass resistance imposed by the DBL has been correlated with nutrient limitation for the giant kelp *Macrocystis pyrifera* [15], and a considerable spatial variation of the DBL over thallus and cryptostomata of *Fucus vesiculosus* has been observed [16]. However, current knowledge of the DBL characteristics of aquatic plants is largely based on point measurements with O_2 microsensors [14], while it is known from boundary layer studies in biofilms [17], corals [18-20] and sediments [17, 21-23] that the DBL exhibits a spatio-temporal heterogeneity, which is modulated by both flow velocity and surface topography. Similar studies of DBL topography are very limited in aquatic plant science [24] and the aim of this study was to explore how the DBL thickness and the local O_2 flux varied spatially over the thallus of *F. vesiculosus* with and without tufts of hyaline hairs. Such first time exploration of the 3D DBL topography was done with O_2 microsensors mounted in a fully automated motorized micromanipulator system that allowed measurements of DBL transects and grids over the thallus of *F. vesiculosus* (Fig. S1). Our results reveal a complex DBL landscape over the algal thallus, where mass transfer across the DBL apparently can be supplemented by advective processes due to the presence of hyaline hairs.

Materials and Methods

Sampling and experimental setup

Specimens of *Fucus vesiculosus* and seawater used in the experimental setup were sampled on the day of usage at <1 m depth at Kronborg, Helsingør, Denmark from May through August. If the influence of a single tuft of hyaline hairs on the DBL was measured, the surface of the thallus surrounding the tuft was carefully shaved off any additional tufts with a scalpel and observation under a dissection microscope to avoid thallus damage. When the influence of multiple tufts was analysed, the thallus was left intact. Prior to measurements, a piece of *F. vesiculosus* thallus with hyaline hairs was fixed on a slab of agar (~1.5% w/w in seawater) in a small flow chamber creating a defined unidirectional flow of seawater across the thallus surface [16]. The flow chamber was connected via tubing to a submersible water pump in a continuously aerated seawater reservoir tank underneath the flow chamber. Flow velocities were adjusted by restricting water flow to the flow chamber, and flow velocity was determined by collecting water from the flow chamber outlet for one minute, where after the sampled volume per time was divided by the cross sectional area of the flow chamber to obtain an estimate of the mean free flow velocity. All measurements were done with flow velocities of either 1.65 cm s^{-1} or 4.88 cm s^{-1}.

The sample was illuminated from above with light from a halogen lamp (Schott KL-2500LCD) equipped with a collimating lens yielding a downwelling photon irradiance (400-700 nm) of ~350 µmol photons m^{-2} s^{-1}, as measured with a quantum irradiance meter (LI-250, LiCor Inc., USA).

Microsensor measurements

Measurements of O_2 concentration above the thallus of *F. vesiculosus* were done with Clark type O_2 microelectrodes (tip diameter 10 µm, OX10, Unisense A/S, Denmark; Revsbech 1989) with a response time of 1-3 seconds and low stirring sensitivity (<2%). The microelectrode was connected to a pA meter (PA2000, Unisense A/S, Denmark) and sensor signals from the pA meter were acquired on a PC via a parallel port -connected A/D converter (ADC-101, Pico Technologies Ltd., England). The O_2 microsensor was mounted in a custom built micromanipulator setup enabling motorized positioning at defined x, y and z coordinates at ~1 µm resolution by use of 3 interconnected motorized

positioners (VT-80, Micos GmbH, Germany) and controllers (MoCo DC, Micos GmbH, Germany). Data acquisition and positioning was controlled by a custom made software (Volfix) programmed in LabView (National Instruments, Japan).

The O_2 microelectrode signal was linearly calibrated at experimental temperature (~17°C) and salinity (S=16) from measurements in air saturated seawater and in seawater made anoxic by addition of sodium dithionite. The O_2 concentration in air saturated seawater, C_0, and the molecular diffusion coefficient of O_2, D_0, in seawater at experimental temperature and salinity was taken from tabulated values (Unisense A/S, Denmark) as $C_0 = 274$ μmol O_2 L^{-1} and $D_0 = 1.87 \cdot 10^{-5}$ cm^2 s^{-1}.

Mapping of diffusive boundary layers

The diffusive boundary layer (DBL) around tufts of hyaline hairs anchored in cryptostomata of *F. vesiculosus* was mapped as 2D transects and 3D grid measurements of O_2 concentration profiles. The Volfix software enabled us to specify a measuring grid/transect with any number of sampling points in the x, y and z-directions. In this study, the y-direction corresponds to the direction of flow (where negative values indicate distance behind a single tuft of hyaline hair), the x-direction corresponds to the width of the flow chamber, and the z-direction corresponds to the height above the thallus surface (Fig. S1). The approximate height and radius of the hyaline hairs was approximated by manual manipulation of the microelectrode tip relative to the structures as observed under a stereomicroscope (SV6, Zeiss, Germany). Thallus samples were placed in the flow chamber with the length of the thallus oriented along the direction of flow, i.e., the y-direction.

2D DBL transects. For 2D transect measurements, the O_2 microelectrode tip was positioned manually as close to the centre of the selected cryptostomata with hyaline hairs as possible using a dissection microscope for observation; this position was set to y=0 in the Volfix measuring software. The transect measurements started 2 mm upstream (y=2 mm) from the cryptostomata and 1 mm above the hyaline hairs (Point A in Fig. S1D), and ended 4 mm downstream (y=-4 mm). Transects of O_2 concentration profiles were measured at a lateral resolution of 0.5 mm in the y-direction, with vertical O_2 concentration profiles done at each transect point in steps of 0.1 mm in the z-direction. All profile measurements started at the same z-position and were finished in the upper

thallus layer, where a characteristic jump in the O_2 concentration, due to the physical impact of the O_2 microsensor and the solid thallus surface, enabled precise determination of the thallus surface.

3D DBL grids. For measuring 3D grids of O_2 concentration profiles over thallus areas with only one tuft of hyaline hairs, 9 transects covering a 24 mm^2 sampling grid area around a central tuft of hairs was set up (Fig. S1E) for O_2 measurements at 0.5 mm lateral resolution (x and y direction) and 0.1 mm vertical resolution (z-direction). Measurements started ~1 mm above the hyaline hairs (Fig. S1E).

For measurements of 3D grids of O_2 concentration profiles over larger thallus areas with multiple tuft of hyaline hairs, an oblong 12 mm by 2 mm measuring grid was set up. Oxygen measurements were done at a lateral resolution of 0.5 mm (x and y directions) and a vertical resolution of 0.2 mm (z direction). Tufts of hyaline hair were scattered across the thallus, and the starting point of the grid measurement was set randomly, but with the same starting point for both the 1.65 cm s^{-1} and 4.88 cm s^{-1} measurements.

Due to the length of measurements different thallus samples were used for individual experiments.

Diffusive boundary layer thickness and calculations

There are different ways of determining the effective thickness of the diffusive boundary layer from O_2 microsensor measurements [17]. The DBL thickness is often found by extrapolating the linear O_2 gradient in the DBL to the bulk concentration of the free-flow region. The distance from the surface to the intersection of the extrapolated linear gradient and the bulk concentration is denoted the effective diffusive boundary layer thickness, Z_δ [3]. However, analysing large numbers of O_2 profiles in this manner is very time consuming, and a somewhat faster determination can be done by defining Z_δ as the distance between the surface and the vertical position above the surface where the O_2 concentration has changed 10% relative to the O_2 concentration in the bulk water. Estimations of Z_δ via this method were found to differ <10% from more precise determinations [17].

The diffusive flux of O_2 across the DBL, J (in units of nmol O_2 cm^{-2} s^{-1}) was calculated from steady state O_2 concentration profiles using Fick's 1st law:

$J = D_0(C_\infty - C_0)/Z_\delta$ (Eq. 1)

where C_∞ is the O_2 concentration in the free-flow region (µmol O_2 L^{-1} = nmol O_2 cm^{-3}), C_0 is the O_2 concentration at the thallus surface (µmol O_2 L^{-1}), Z_δ is the effective DBL thickness (cm), and D_0 is the molecular diffusion coefficient of O_2 in seawater (cm^2 s^{-1}). To compensate for the uneven surface of thalli, measurements below the thallus surface are not shown on final transects. The depth axis on transects is therefore denoted $z' = z - z_0$, where z is the z-coordinate from the sample data, and z_0 is the z-coordinate of the thallus surface. The thallus surface position was determined from the intermittent sudden drop in O_2 concentration when the microsensor pushed against the thallus surface cortex. Maps of O_2 concentration, Z_δ, and J were generated from measured transects and grids using data interpolation software (Kriging gridding method using default settings, i.e. Linear Variogram and Point Kriging, Surfer v.8, Golden Software Inc., USA).

Statistics

Two-way ANOVAs were applied to test differences in the mean Z_δ over *F. vesiculosus* between flow rates and light conditions (light/dark). For significant main effects (flow rate and/or light condition) and interaction effects, Tukey's multiple comparisons post hoc test was applied. Two-way ANOVAs were applied to test differences between mean O_2 flux values between flow rates and thallus condition (single or multiple tufts). For significant main effects (flow rate and/or thallus condition) and interaction effects, Tukey's multiple comparisons post hoc test was applied. Statistical analysis was performed using Rstudio (Rstudio version 0.99.491, 2016) with the level of significance set to $p < 0.05$.

Results

The DBL around single tufts of hyaline hairs

Isopleths of O_2 concentration in the water column above the thalli showed a local increase in effective DBL thickness, Z_δ associated with the hyaline hair tuft (Fig. 1), with highest Z_δ values located downstream from the hyaline hairs, either directly behind the tuft or even within the expanse of the hyaline hairs. In light (350 µmol photons m^{-2} s^{-1}), and at a flow of 1.65 cm s^{-1}, Z_δ reached a maximum thickness of 1.2 mm downstream relative to

the tuft at y = -0.5 mm (Fig. S2, S3A), while under a flow of 4.88 cm s^{-1}, the maximum Z_δ was reduced to 0.6 mm at y = -2.5 mm (Fig. S3A). In darkness, the maximal Z_δ values were 0.9 mm and 0.4 mm at y = -2 mm and y = 0 mm under flows of 1.65 and 4.88 cm s^{-1}, respectively. The mean Z_δ did not change significantly ($p<0.05$) between measurements in light and darkness (Fig. S3B) under low flow ($Z_{\delta(Light)}$ = 0.72 mm, $Z_{\delta(Dark)}$ = 0.58 mm; p adj = 0.26) or high flow ($Z_{\delta(Light)}$ = 0.36 mm, $Z_{\delta(Dark)}$ = 0.18 mm; p adj = 0.13). However, flow velocity had a significant effect on the mean Z_δ that was significantly thinner under high flow (4.88 cm s^{-1}) as compared to the low flow (1.65 cm s^{-1}) (p adj < 0.001 for both main effects).

The hyaline hairs affected Z_δ downstream from the hair tuft (Fig. 1A,B) causing a thickening of the DBL that also expanded perpendicular to the flow direction (Fig. 1C,D), reaching a maximum expansion at y = -2 mm at both flows ($Z_{\delta Max}$= 1.8 mm for 1.65 cm s^{-1} and $Z_{\delta Max}$=0.9 mm for 4.88 cm s^{-1}). Beyond the local peak in boundary layer thickness, the DBL closely followed the contours of the thallus surface topography. Two transects measured at higher resolution along the x-axis at y=-2 mm showed that the increase in Z_δ was roughly identical and extended ~1 mm on both sides of the hyaline hair tuft (Fig. 1C,D). At distances >1 mm away from the local maximum, the DBL thickness approached a lower more homogeneous DBL thickness over thallus areas unaffected by the hair tuft.

Unexpectedly, a transect of O_2 concentrations above the illuminated thallus at y= -2 mm in the x direction, i.e., perpendicular to the flow, showed a local O_2 increase followed by a decrease in oxygen concentration that was apparently independent of Z_δ (Fig. 1C). A longitudinal transect at x=-0.5 mm along the y-direction, i.e., the flow direction, showed further indications of an apparent local "upwelling" of O_2 into the transition zone between the DBL and the fully mixed water column protruding downstream from the hyaline hair tuft (Fig. 2). We found such "upwelling" zones most pronounced under low flow located ~2 mm downstream from the centre of the tuft and extending several mm into the water column with O_2 concentrations reaching up to >2 times air saturation in some cases (Fig. 2A).

The DBL around multiple tufts of hyaline hairs

3D grid measurements of O_2 concentration over a *F. vesiculosus* thallus with several tufts of hyaline hairs spaced at approximately 2-5 mm distance were done to investigate potential combined effects of multiple tufts on the DBL. Such measurements showed that the smooth local thickening of the DBL around a single hyaline tuft relative to the DBL of the smooth thallus was altered in the presence of multiple tufts (Fig. 3). The DBL topography was more heterogeneous with Z_δ varying >1 mm reaching a maximum thickness of >2.5 mm under low flow and >1.5 mm under high flow, respectively. The DBL topography was apparently largely determined by the interaction between flow and the tufts of hyaline hairs under low flow, while the smooth thallus surface topography led to local minima in Z_δ in-between individual tufts at higher flow velocity (Fig. 3B).

Transects of O_2 concentrations at x=1 mm (extracted from the 3D grids in Fig. 3A,B) gave a detailed information on how O_2 concentration varied over the thallus with distance along the thallus in the flow direction (Fig. 3C,D). In light, the thallus surface O_2 concentration reached >900 µM in both flows, while the O_2 concentration in the transient zone of the DBL (z=0.7 mm) varied between 350 and 750 µM under low flow and between 300 and 550 µM in high flow, respectively, clearly demonstrating a compression of the boundary layer and more effective O_2 exchange between thallus and water under higher flow.

However, the thickening of the 300-350 µM O_2 contour areas e.g. at y=-11 mm and y=-6 mm (Fig. 3C) was due to gradual increasing O_2 concentrations from the bulk water towards the upper part of the DBL (data not shown). This creates an artefact in the precise determination of Z_δ by the method proposed by Jørgensen and Des Marais [17] that will overestimate the local DBL thickness e.g. compared to the local profile in y=-1 mm where a more steady O_2 increase was measured.

Diffusive O_2 fluxes over the *Fucus* thallus with single and multiple tufts

Although inconsistencies were found (e.g. in the area around x = -1.5 mm, y = 1.5mm in Fig. 4A,B), increases in DBL thickness generally correlated with a decrease in O_2 flux, and the flow-dependent DBL topography strongly affected the O_2 flux from the illuminated *F. vesiculosus* thallus.

296 Comparing the O_2 fluxes in transects over the *F. vesiculosus* thallus with single and
297 multiple tufts of hyaline hairs (Fig. 5A,B) showed an increased O_2 flux just upstream to
298 the position of the hyaline hair tufts independent of the flow velocity. The flux values
299 generally correlated with the DBL thickness and the flux gradually decreased downstream
300 relative to the hair tuft. However, some local variations were seen in areas exhibiting less
301 uniform increases in O_2 concentration towards the thallus surface.
302 The average O_2 flux calculated from transects over *F. vesiculosus* thalli with single and
303 multiple hyaline hair tufts (Fig. 5C,D) showed that flow was the major determinant of gas
304 exchange between macroalga and the surrounding seawater. Both in measurements over
305 single and multiple hair tufts, the O_2 flux values were higher in high flow treatments as
306 compared to low flow (p adj <0.001). The O_2 fluxes measured around a single hair tuft
307 under high flow were higher than the corresponding measurements over multiple tufts
308 treatment (Fig. 5C,D; p adj <0.001). However, the flux values in the multiple tuft
309 treatments were averaged over a two times larger distance (Fig. 5C; 12 mm), and thus
310 include the combined effect of multiple tufts and DBL variation over these, while the
311 values of the single tuft treatments (Fig. 5D; 6mm) only reflect the DBL effects on O_2
312 flux immediately downstream from the hair tuft.
313
314 **Discussion**
315 In our measurements around single tufts of hyaline hairs, the DBL followed the contour
316 of the smooth thallus surface, except around the hair tufts where a thickening occurred
317 downstream of tufts and perpendicular to the flow direction, with a concomitant decrease
318 in the thickness 1-2 mm away from the hair tufts, depending on the flow-regime.
319 In measurements over multiple tufts, the smooth thickening of the DBL observed around
320 isolated single tufts was absent. This more dynamic DBL landscape is probably caused
321 by the close vicinity of neighbouring hyaline hair tufts, where the DBL thickness between
322 tufts never reach 'normal' conditions over a smooth thallus. Interestingly, this suggests
323 that the effect of multiple hair tufts overall increased the DBL thickness across the thallus.
324 Intuitively, a thin boundary layer would create physical conditions that could better avoid
325 high detrimental O_2 concentrations and inorganic carbon limitations in light and O_2
326 limitation in darkness. So why does *Fucus* spend metabolic energy on production of
327 hyaline hairs? In early work by Raven [11], it was suggested that hyaline hairs aid in

328 nutrient uptake by having a highly decreased diffusion resistance over the plasmalemma
329 compared to the thick algal thallus, and in addition the hairs could protrude through the
330 viscous sublayer and into the mainstream flow with better nutrient access. However, as
331 pointed out by Hurd [14], the thin and flexible hairs are considered unlikely to disrupt the
332 viscous sublayer and create turbulence themselves. Here we show that across a thallus
333 with multiple hair tufts, the overall DBL thickness is increased, which has a functional
334 significance similar to observed DBL effects of epiphytes on submerged macrophytes
335 [24, 25]. The thickening of the boundary layer thickness creates a mass transfer limitation
336 that in light can lead to high O_2 concentrations [24, 26] potentially inducing
337 photorespiration [27] and limiting the inorganic carbon supply [28] to the thallus.
338 However, such mass transfer limitation would also maintain higher nutrient
339 concentrations due to surface-associated enzyme activity that can aid in the uptake of e.g.
340 phosphorous and other nutrients [14, 29].
341 A thicker diffusive boundary layer over thalli with tufts of hyaline hairs could also create
342 a niche for epibiotic bacteria, and the presence of bacteria on algal thalli is well known
343 [30-32]. In light of the recently developed 'holobiont' concept [32, 33] a physical
344 structure that would keep the algal associated bacteria more protected and provide them
345 with metabolic compounds, could present a competitive advantage. Studies of the role of
346 bacteria in algal life-cycle and metabolism have shown that a strong host specificity of
347 epiphytic bacterial communities exists, possibly shaped by the algal metabolites as the
348 primary selective force [34]. Previous studies have e.g. demonstrated the presence of N_2
349 fixing cyanobacteria as part of the algal microbiome, and it has also been shown that
350 native bacteria are required for normal morphological development in some algae [35].
351 However, the actual distribution and ecological niches of such macroalgae-associated
352 microbes are not well studied. Spilling et al. (2010) found more pronounced O_2 dynamics,
353 reaching anoxia during darkness, in the cryptostomata cavities of *F. vesiculosus*, wherein
354 the hyaline hairs are anchored. Cryptostomata could thus represent potential niches for
355 bacterial aerobic and anaerobic degradation of organic substrates or O_2-sensitive N_2
356 fixation that warrant further exploration.
357 In some DBL transects measured on light exposed *Fucus* thalli, we observed areas of
358 enhanced O_2 concentration detached from the boundary layer (Fig. 2). In a previous study,
359 it was shown that nutrient uptake rates could increase 10-fold when the boundary layer

was periodically stripped by passing waves [36]. However, in our case the flow upstream from the tuft was laminar and no waves or DBL stripping occurred. The observed phenomenon of enhanced O_2 above the DBL could be explained by a combination of factors. As flow is obstructed by a physical object a differential pressure field is created where a local drop in pressure is created around the hyaline hairs due to the locally smaller cross section of unobstructed flow. Such pressure gradient could create a local advective upwelling around the area of low pressure thus affecting the O_2 transport. The phenomena is well described in e.g. sediment transport [37] and plumes of O_2 release have also been observed before in coral-reef-associated algae *Chaetomorpha sp.* using planar optodes [38].

In addition, so-called vortex shedding (von Kármán vortex sheets) could also be a factor influencing the observed O_2 release. Shedding of vortices can occur at certain Reynold numbers at the transition between laminar and turbulent flow when the pressure increases in the direction of the flow, i.e., in the presence of a so-called adverse pressure gradient [39]. In our study, the flow upstream from the hyaline hairs was laminar but a transition to turbulent flow can occur, even at low Reynold numbers, when a certain surface roughness is present and vortex shedding can initiate at Reynold numbers of ~50 [40]. Using characteristic scales from this study (hyaline hair tuft diameter = 2 mm; free-stream velocity = 1.65 or 4.88 cm s^{-1}; fluid density = 1 kg L^{-1} and a dynamic fluid viscosity of 1.08×10^{-3} Pa s [41], we calculated Reynold numbers of ~30-90. Von Kármán vortices have previously been connected to flow patterns on the lee side of plant parts [42] and based on the calculated Reynold numbers the theoretical basis for generation of vortex shedding [40] due to tufts of hyaline hairs is present in our experimental setup.

We thus speculate that a combination of pressure gradient mediated upwelling of O_2 and vortex shedding (Fig. 6) could explain the observed phenomena in Fig. 2. The local mass transfer related to the presence of hyaline hair tufts on Fucoid macroalgae may thus be more complex. A more detailed investigation of such phenomena was beyond the scope of the present study and would clearly require more detailed characterization of the hydrodynamic regimes over thalli with and without tufts of hyaline hairs.

In conclusion, our study of the chemical boundary layer landscape over the thallus of *F. vesiculosus* revealed a strong local effect on the DBL over and around tufts of hyaline hairs anchored in cryptostomata. Single tufts showed a thickening of the DBL

392 downstream and horizontally relative to the thinner DBL over the smooth thallus surface,
393 while areas with multiple tufts exhibited a consistently thickened DBL that may affect
394 gas and nutrient exchanges between the alga and seawater. Furthermore, we also observed
395 more complex solute exchange phenomena that were apparently driven by pressure
396 gradients and/or vortex shedding over the hyaline hair tufts. Altogether, this study
397 demonstrates that interactions between flow and distinct macroalgal surface topography
398 gives rise to local heterogeneity in the chemical landscape and solute exchange that may
399 allow for microenvironmental niches harbouring microbial epiphytes facilitating a
400 diversity of aerobic and anaerobic processes. Further microscale studies of such niches in
401 combination with e.g. microscopy and molecular detection of microbes in relation to
402 hyaline hairs and cryptostomata thus seem an important next step to reveal further insights
403 to the presence and role of the microbiome of Fucoid algae.
404

405 **Acknowledgements**

406 This study was supported by grants from the Danish Council for Independent Research |
407 Natural Sciences (MK), and a PhD stipend from the Department of Biology, University
408 of Copenhagen (ML). We thank Roland Thar (Pyro-Science GmbH) for his help in
409 establishing the 3D microsensor measurement setup and software and Erik Trampe for
410 help with photography of Fig. S1C. The authors declare no conflict of interest and no
411 competing financial interest.
412

413 **Author contributions**

414 RDN and MK designed the research, RDN and ML performed the research, ML, RDN
415 and MK analysed data, ML wrote the paper with editorial assistance from RDN and MK.
416 All authors gave final approval for publication.

References

[1] Sand-Jensen, K. & Krause-Jensen, D. 1997 Broad-scale comparison of photosynthesis in terrestrial and aquatic plant communities. *Oikos* **80**, 203-208. (doi:Doi 10.2307/3546536).

[2] Maberly, S.C. & Madsen, T.V. 2002 Freshwater angiosperm carbon concentrating mechanisms: processes and patterns. *Funct Plant Biol* **29**, 393-405. (doi:10.1071/Pp01187).

[3] Jørgensen, B.B. & Revsbech, N.P. 1985 Diffusive boundary-layers and the oxygen-uptake of sediments and detritus. *Limnol Oceanogr* **30**, 111-122.

[4] Glud, R.N., Gundersen, J.K., Revsbech, N.P. & Jørgensen, B.B. 1994 Effects on the benthic diffusive boundary-layer imposed by microelectrodes. *Limnol Oceanogr* **39**, 462-467.

[5] Lorenzen, J., Glud, R.N. & Revsbech, N.P. 1995 Impact of microsensor-caused changes in diffusive boundary-layer thickness on O_2 profiles and photosynthetic rates in benthic communities of microorganisms. *Mar Ecol Prog Ser* **119**, 237-241. (doi:DOI 10.3354/meps119237).

[6] Black, M.A., Maberly, S.C. & Spence, D.H.N. 1981 Resistances to carbon dioxide fixation in four submerged freshwater macrophytes. *New Phytologist* **89**, 557-568.

[7] Pedersen, O. & Colmer, T.D. 2014 Underwater photosynthesis and internal aeration of submerged terrestrial wetland plants. In *Low-oxygen stress in plants - Oxygen sensing and adaptive responses to hypoxia* (eds. J.T. van Dongen & F. Licausi), pp. 315-327. Wien, Austria, Springer Verlag.

[8] Pedersen, O., Colmer, T.D. & Sand-Jensen, K. 2013 Underwater photosynthesis of submerged plants - recent advances and methods. *Frontiers in Plant Science* **4**, 140. (doi:10.3389/fpls.2013.00140).

[9] Shapiro, O.H., Fernandez, V.I., Garren, M., Guasto, J.S., Debaillon-Vesque, F.P., Kramarsky-Winter, E., Vardi, A. & Stocker, R. 2014 Vortical ciliary flows actively enhance mass transport in reef corals. *Proceedings of the National Academy of Sciences* **111**, 13391-13396. (doi:10.1073/pnas.1323094111).

[10] Hurd, C.L., Galvin, R.S., Norton, T.A. & Dring, M.J. 1993 Production of hyaline hairs by intertidal species of *Fucus* (Fucales) and their role in phosphate-uptake. *J Phycol* **29**, 160-165. (doi:DOI 10.1111/j.0022-3646.1993.00160.x).

[11] Raven, J.A. 1981 Nutritional strategies of submerged benthic plants - the acquisition of C, N and P by rhizophytes and haptophytes. *New Phytologist* **88**, 1-30.

[12] Steen, H. 2003 Apical hair formation and growth of *Fucus evanescens* and *F. serratus* (Phaeophyceae) germlings under various nutrient and temperature regimes. *Phycologia* **42**, 26-30. (doi:DOI 10.2216/i0031-8884-42-1-26.1).

[13] Oates, B.R. & Cole, K.M. 1994 Comparative studies on hair cells of two agarophyte red algae, *Gelidium vagum* (Gelidiales, Rhodophyta) and *Gracilaria pacifica* (Gracilariales, Rhodophyta). *Phycologia* **33**, 420-433. (doi:doi:10.2216/i0031-8884-33-6-420.1).

[14] Hurd, C.L. 2000 Water motion, marine macroalgal physiology, and production. *J Phycol* **36**, 453-472. (doi:DOI 10.1046/j.1529-8817.2000.99139.x).

[15] Wheeler, W.N. 1980 Effect of boundary-layer transport on the fixation of carbon by the giant-kelp *Macrocystis pyrifera*. *Mar Biol* **56**, 103-110. (doi:Doi 10.1007/Bf00397128).

462 [16] Spilling, K., Titelman, J., Greve, T.M. & Kühl, M. 2010 Microsensor
463 measurements of the external and internal microenvironment of *Fucus vesiculosus*
464 (Phaeophyceae). *J Phycol* **46**, 1350-1355. (doi:DOI 10.1111/j.1529-
465 8817.2010.00894.x).
466 [17] Jørgensen, B.B. & Des Marais, D.J. 1990 The diffusive boundary layer of
467 sediments - Oxygen microgradients over a microbial mat. *Limnol Oceanogr* **35**, 1343-
468 1355.
469 [18] Kühl, M., Cohen, Y., Dalsgaard, T., Jørgensen, B.B. & Revsbech, N.P. 1995
470 Microenvironment and photosynthesis of zooxanthellae in scleractinian corals studied
471 with microsensors for O_2, pH and light. *Mar Ecol Prog Ser* **117**, 159-172.
472 [19] de Beer, D., Kühl, M., Stambler, N. & Vaki, L. 2000 A microsensor study of light
473 enhanced Ca2+ uptake and photosynthesis in the reef-building hermatypic coral *Favia*
474 *sp. Mar Ecol Prog Ser* **194**, 75-85.
475 [20] Jimenez, I.M., Kuhl, M., Larkum, A.W.D. & Ralph, P.J. 2011 Effects of flow and
476 colony morphology on the thermal boundary layer of corals. *J R Soc Interface* **8**, 1785-
477 1795. (doi:10.1098/rsif.2011.0144).
478 [21] Gundersen, J.K. & Jørgensen, B.B. 1990 Microstructure of diffusive boundary
479 layers and the oxygen uptake of the sea floor. *Nature* **345**, 604-607.
480 [22] Røy, H., Hüttel, M. & Jørgensen, B.B. 2002 The role of small-scale sediment
481 topography for oxygen flux across the diffusive boundary layer. *Limnol Oceanogr* **47**,
482 837-347.
483 [23] Røy, H., Hüttel, M. & Jørgensen, B.B. 2005 The influence of topography on the
484 functional exchange surface of marine soft sediments, assessed from sediment
485 topography measured *in situ*. *Limnol Oceanogr* **50**, 106-112.
486 [24] Brodersen, K.E., Lichtenberg, M., Paz, L.-C. & Kühl, M. 2015 Epiphyte-cover on
487 seagrass (*Zostera marina* L.) leaves impedes plant performance and radial O_2 loss from
488 the below-ground tissue. *Frontiers in Marine Science* **2:58**.
489 (doi:10.3389/fmars.2015.00058).
490 [25] Sand-Jensen, K., Revsbech, N.P. & Jørgensen, B.B. 1985 Microprofiles of oxygen
491 in epiphyte communities on submerged macrophytes. *Mar Biol* **89**, 55-62. (doi:Doi
492 10.1007/Bf00392877).
493 [26] Lichtenberg, M. & Kühl, M. 2015 Pronounced gradients of light, photosynthesis
494 and O_2 consumption in the tissue of the brown alga *Fucus serratus*. *New Phytologist*
495 **207**, 559-569. (doi:10.1111/nph.13396).
496 [27] Falkowski, P. & Raven, J.A. 2007 *Aquatic photosynthesis. 2. Edition*. 2 ed.
497 Princeton, USA, Princeton University Press.
498 [28] Larkum, A.W.D., Koch, E.M.W. & Kühl, M. 2003 Diffusive boundary layers and
499 photosynthesis of the epilithic algal community of coral reefs. *Mar Biol* **142**, 1073-
500 1082. (doi:DOI 10.1007/s00227-003-1022-y).
501 [29] Raven, J.A. 1992 How benthic macroalgae cope with flowing fresh-water -
502 resource acquisition and retention. *J Phycol* **28**, 133-146. (doi:DOI 10.1111/j.0022-
503 3646.1992.00133.x).
504 [30] Cundell, A.M., Sleeter, T.D. & Mitchell, R. 1977 Microbial populations associated
505 with the surface of the brown alga *Ascophyllum nodosum*. *Microbial Ecol* **4**, 81-91.
506 [31] Bolinches, J., Lemos, M.L. & Barja, J.L. 1988 Population dynamics of
507 heterotrophic bacterial communities associated with *Fucus vesiculosus* and *Ulva rigida*
508 in an estuary. *Microbial Ecol* **15**, 345-357. (doi:10.1007/bf02012647).

509 [32] Egan, S., Harder, T., Burke, C., Steinberg, P., Kjelleberg, S. & Thomas, T. 2013
510 The seaweed holobiont: understanding seaweed-bacteria interactions. *Fems Microbiol*
511 *Rev* **37**, 462-476. (doi:Doi 10.1111/1574-6976.12011).
512 [33] Bordenstein, S.R. & Theis, K.R. 2015 Host biology in light of the microbiome: Ten
513 principles of holobionts and hologenomes. *PLoS Biology* **13**, e1002226.
514 (doi:10.1371/journal.pbio.1002226).
515 [34] Lachnit, T., Blumel, M., Imhoff, J.F. & Wahl, M. 2009 Specific epibacterial
516 communities on macroalgae: phylogeny matters more than habitat. *Aquat Biol* **5**, 181-
517 186. (doi:10.3354/ab00149).
518 [35] Provasoli, L. & Pintner, I.J. 1980 Bacteria induced polymorphism in an axenic
519 laboratory strain of *Ulva Lactuca* (Chlorophyceae). *J Phycol* **16**, 196-201. (doi:DOI
520 10.1111/j.1529-8817.1980.tb03019.x).
521 [36] Stevens, C.L. & Hurd, C.L. 1997 Boundary-layers around bladed aquatic
522 macrophytes. *Hydrobiologia* **346**, 119-128. (doi:Doi 10.1023/A:1002914015683).
523 [37] Huettel, M., Ziebis, W. & Forster, S. 1996 Flow-induced uptake of particulate
524 matter in permeable sediments. *Limnol Oceanogr* **41**, 309-322.
525 [38] Haas, A.F., Gregg, A.K., Smith, J.E., Abieri, M.L., Hatay, M. & Rohwer, F. 2013
526 Visualization of oxygen distribution patterns caused by coral and algae. *PeerJ* **1**, e106.
527 (doi:10.7717/peerj.106).
528 [39] Bearman, P.W. 1984 Vortex shedding from oscillating bluff bodies. *Annual Review*
529 *of Fluid Mechanics* **16**, 195-222.
530 [40] Nepf, H.M. 1999 Drag, turbulence, and diffusion in flow through emergent
531 vegetation. *Water Resources Research* **35**, 479-489. (doi:10.1029/1998wr900069).
532 [41] Kaye, G.W.C. & Laby, T.H. 1995 *Tables of Physical & Chemical Constants (16th*
533 *Edition)*. 16 ed.
534 [42] Nikora, V. 2010 Hydrodynamics of aquatic ecosystems: An interface between
535 ecology, biomechanics and environmental fluid mechanics. *River Research and*
536 *Applications* **26**, 367-384. (doi:10.1002/rra.1291).

Figure legends

Figure 1. Fine-scale mapping of DBL around a single tuft of hyaline hairs on an illuminated *Fucus vesiculosus* thallus (350 µmol photons m^{-2} s^{-1}). (A) and (B) 3D plots of *F. vesiculosus* thallus surface (grey area) and upper extension of DBL (coloured area) around a single tuft of hyaline hairs, at flow velocities of 1.65 (left panels) and 4.88 cm s^{-1} (right panels). Colour bars depict the effective DBL thickness, Z_δ (mm), and arrows indicate the direction of flow. (C) and (D) Transects in the x-direction (perpendicular to the flow), at position y=-2 mm from Fig. 1 A,B, respectively, normalized to thallus surface showing the local O_2 concentration. The zero position (0,0) indicates the position of the cryptostomata. Colour bars denote O_2 concentration (in µmol O_2 L^{-1}). (E) and (F) Transects of O_2 concentration (in µmol L^{-1}) measured across a single tuft of hyaline hairs in *Fucus vesiculosus* measured at flow velocities of 1.65 (E) and 4.88 cm s^{-1} (F), in light (350 µmol photons m^{-2} s^{-1}). The arrows indicate flow direction. The zero position (0,0) indicates the position of the cryptostomata, and transects were adjusted to the thallus surface. Colour bars denote O_2 concentration (in µmol O_2 L^{-1}).

Figure 2. Local transects of O_2 concentration around single hair tufts from two different measurement series over an illuminated *Fucus vesiculosus* thallus (350 µmol photons m^{-2} s^{-1}). (A) shows a transect taken from Fig. 1A at x=-0.5 under a flow velocity of 1.65 cm s^{-1}, while (B) was measured similarly as Fig. 1E, also at a flow velocity of 1.65 cm s^{-1}. The hair tufts were 2.5-3 mm in diameter and protruded 3-3.5 mm from the thallus. Both transects were adjusted to the thallus surface. The black arrow indicates the flow direction. Colour bars denote O_2 concentration (in µmol O_2 L^{-1}).

Figure 3. Mapping of DBL over several tufts of hyaline hairs on an illuminated *Fucus vesiculosus* thallus (350 µmol photons m^{-2} s^{-1}). (A) and (B) 3D plot of *F. vesiculosus* thallus surface (grey area) and the upper extension of the DBL (coloured area) of multiple tufts of hyaline hairs under a flow velocity 1.65 (left panels) and 4.88 cm s^{-1} (right panels). Colour bars depict the effective DBL thickness, Z_δ (mm). (C) and (D) Transects of O_2 concentration at position x=1 (along the y-axis direction) normalized to thallus surface. Colour bars denote O_2 concentration (in µmol O_2 L^{-1}).

Figure 4. Isopleths of O_2 flux (in nmol O_2 cm^{-2} s^{-1}) (A) and (C) and effective DBL thickness, Z_δ (in mm) (B) and (D) measured over an illuminated *Fucus vesiculosus* thallus (350 µmol photons m^{-2} s^{-1}) around a single tuft of hyaline hairs at flow velocities of 1.65 cm s^{-1} (A, B) and 4.88 cm s^{-1} (C, D). The hyaline hairs were rooted in the cryptostomata located at the (0,0) coordinate, as indicated by the black cross. Black arrows indicate the flow direction.

Figure 5. Comparison of O_2 flux values (in nmol O_2 cm^{-2} s^{-1}) calculated from transects of O_2 concentration profiles measured over an illuminated (350 µmol photons m^{-2} s^{-1}) intact *Fucus vesiculosus* thallus with several tufts of hyaline hairs (A) and a thallus with only a single hair tuft (B) measured under flow velocities of 1.65 cm s^{-1} and 4.88 cm s^{-1}. Note the difference in x-scale. The black arrow indicates the flow direction. The individual position of the multiple hairtufts in panel (A) were not mapped and the zero position on the x-axis thus only reflects the starting point of the transect. In panel (B), the zero position indicates the centre of the cryptostomata. Panel (C) and (D) show the average O_2 flux (±SEM) across (C) the intact thallus and (D) the thallus with a single hair tuft protruding.

Figure 6. Conceptual drawing showing possible scenarios for the observed upwelling of O_2 downstream of the hyaline hairs. Flow velocity (straight black lines) decreases from the free stream velocity as the thallus surface is approached through the diffusive boundary layer (DBL). The hyaline hair tuft protruding from cryptostomata alters the DBL thickness locally and creates a differential pressure field (shown in gradient blue and red colours) due to the smaller cross section of unobstructed flow. This creates a flow acceleration in the areas of relative low pressure which could result in advective upwelling. In addition, an adverse pressure gradient is generated downstream from the hair tuft potentially resulting in vortex shedding.

537

Figures

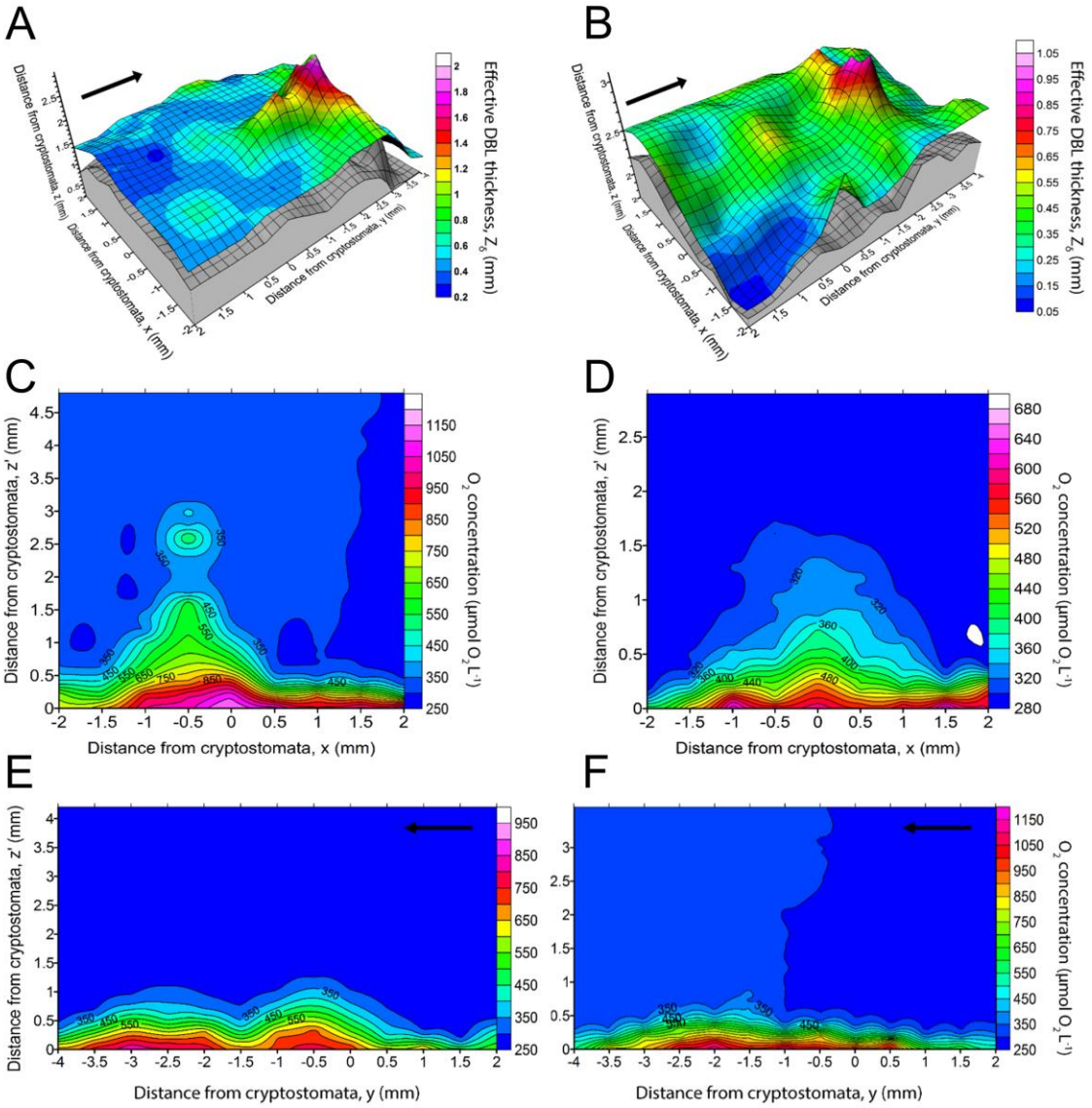

Figure 1

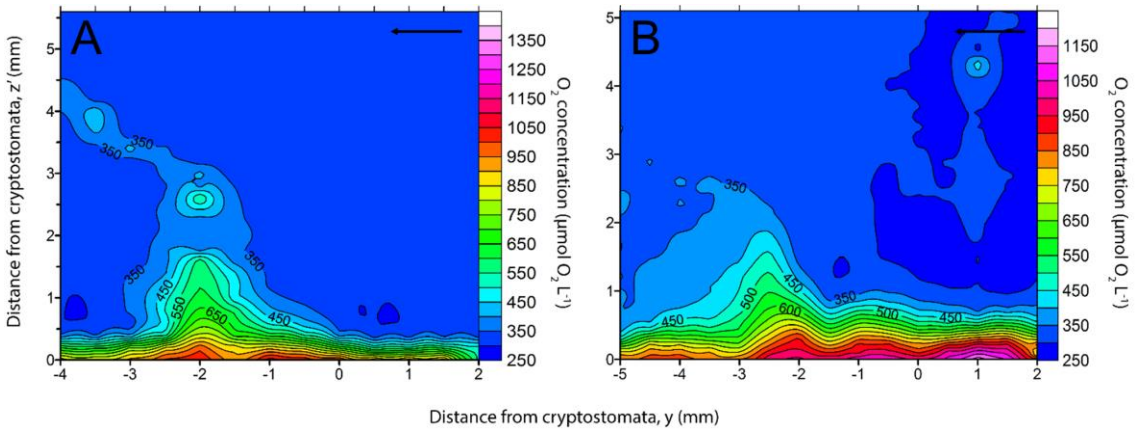

Figure 2

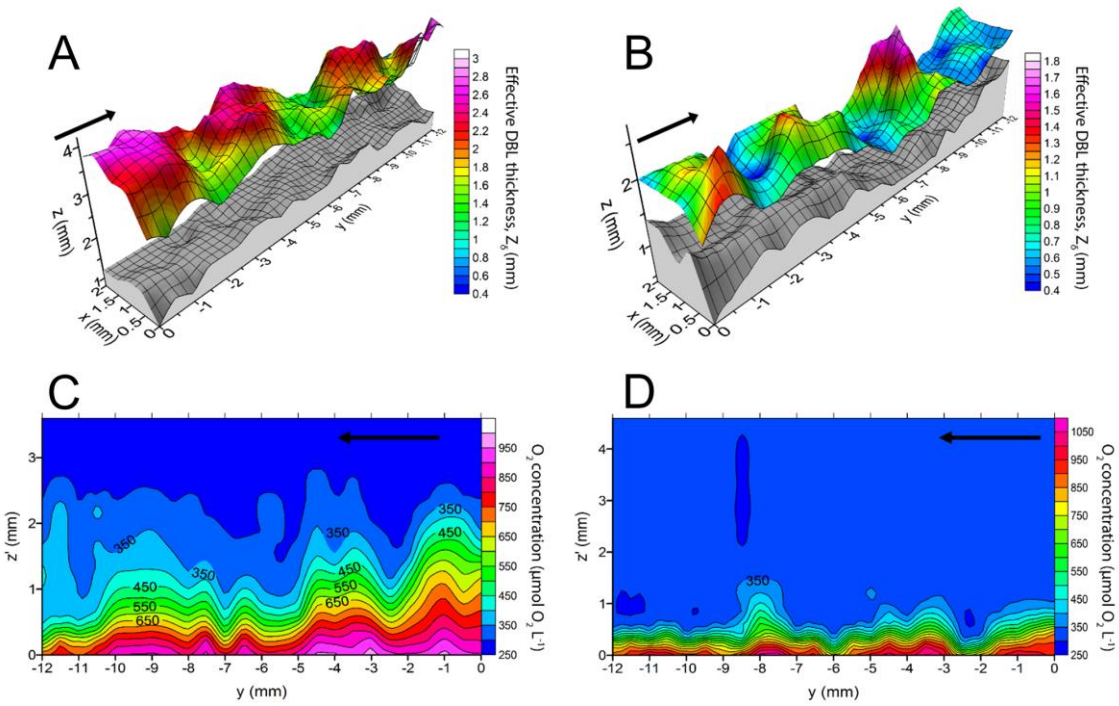

Figure 3

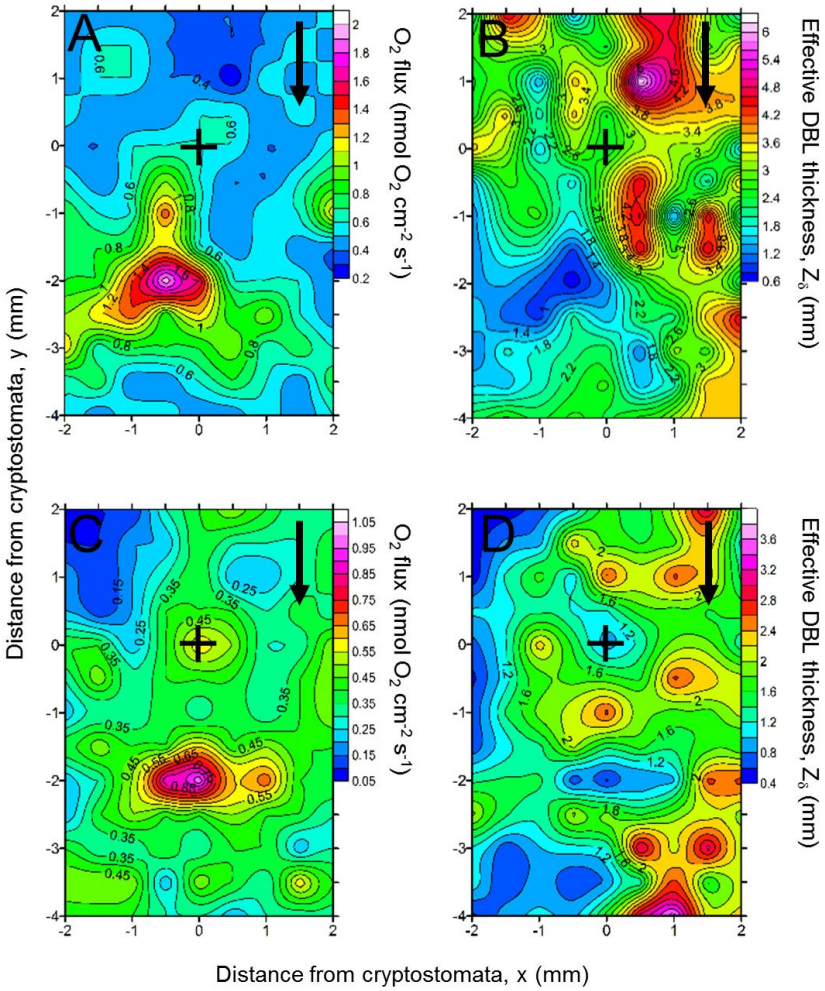

Figure 4

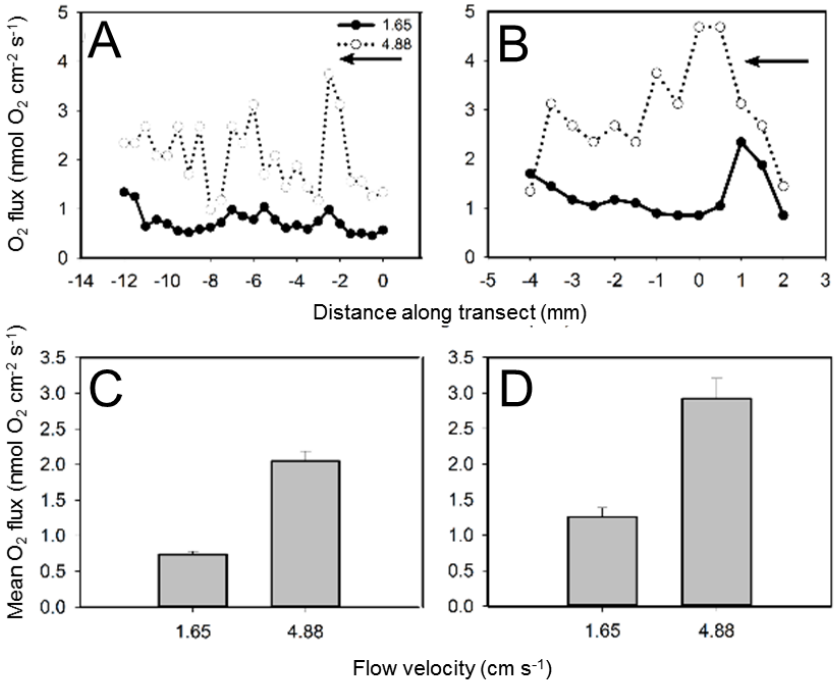

Figure 5

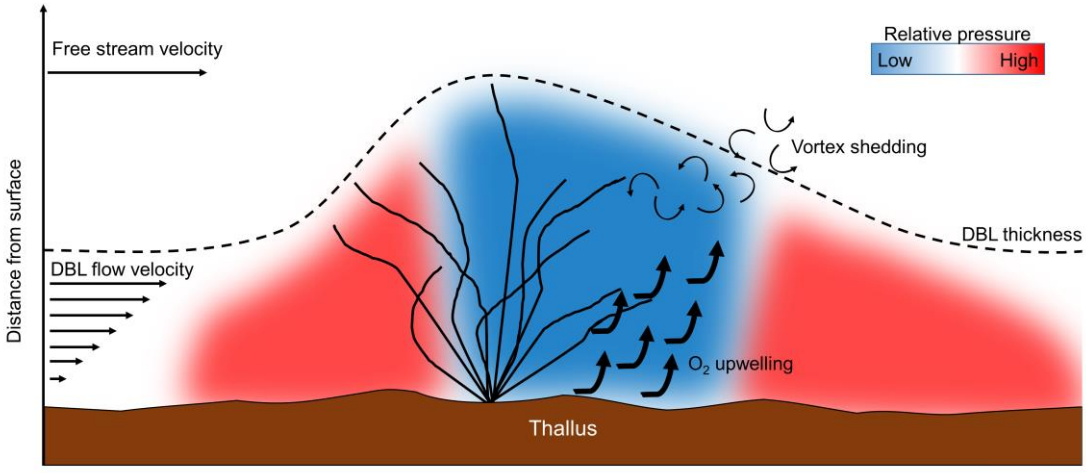

Figure 6